CrossMark

Realization of a gain with electromagnetically induced transparency system using non-degenerate Zeeman sublevels in ^{87}Rb

Minchuan Zhou [a],*, Zifan Zhou [b], Selim M. Shahriar [a,b]

[a] Department of Physics and Astronomy, Northwestern University, Evanston, IL 60208, USA
[b] Department of EECS, Northwestern University, Evanston, IL 60208, USA

ARTICLE INFO

ABSTRACT

Previously, we had proposed an optically-pumped five-level Gain EIT (GEIT) system, which has a transparency dip superimposed on a gain profile and exhibits a negative dispersion suitable for the white-light-cavity signal-recycling (WLC-SR) scheme of the interferometric gravitational wave detector (Zhou et al., 2015). Using this system as the negative dispersion medium (NDM) in the WLC-SR, we get an enhancement in the quantum noise (QN) limited sensitivity-bandwidth product by a factor of ∼18. Here, we show how to realize this GEIT system in a realistic platform, using non-degenerate Zeeman sublevels in cold Rb atoms, employing anomalous dispersion at 795 nm. Using the Caves model for a phase insensitive linear amplifier, we show that an enhancement of the sensitivity-bandwidth product by a factor of ∼17 is possible for potentially realizable experimental parameters. While the current LIGO apparatus uses light at 1064 nm, a future embodiment thereof may operate at a wavelength that is consistent with the wavelength considered here.

© 2017 Elsevier B.V. All rights reserved.

1. Introduction

A white light cavity (WLC) [1–7] is an optical cavity that contains a dispersive medium and resonates over a broader range of frequencies compared to an empty cavity and still maintains a high buildup factor. Consider, for example, a ring cavity, for which the resonance condition is met when its length is an integer multiple of the wavelength, and the width of the resonance is determined by the reflectivity of the mirrors. When a negative dispersion medium inserted in the cavity is tuned to the condition under which the wavelength does not change with frequency for a range around the resonance of the empty cavity, the cavity will resonate over this range without any increase in the cavity loss.

Previously, we had presented an interferometric gravitational wave (GW) detector using a WLC for signal recycling (the WLC-SR scheme) [8]. The key element in this scheme is a negative dispersion medium (NDM), with vanishingly small additional noise, used to compensate the phase variation due to change in frequency, including optomechanical effects. One candidate medium for realizing the NDM makes use of a pair of adjacent Lorentzian gain peaks generated by exciting a Raman transition with two non-degenerate pumps. When the two gain peaks are brought close enough to produce the slope in negative dispersion required for the phase compensation, the gain in the center dip becomes so large that lasing occurs, and the system

becomes unstable [9]. We showed in Ref. [8] that this constraint can be circumvented by using the so-called GEIT system for realizing the negative dispersion. Specifically, the GEIT system uses five energy levels in the M-configuration to produce gain with electromagnetically induced transparency [8]. The quantum noise from this configuration was evaluated rigorously using the master equation (ME) approach [10] in our numerical simulation. The resulting sensitivity-bandwidth product (defined as the product of the highest sensitivity determined by the minimum QN and the bandwidth determined by the full width at twice the minimum QN) is enhanced by a factor of ∼18 [8] compared to the highest sensitivity result predicted by Buonanno and Chen [11]. To the best of our knowledge, such a GEIT system has not been studied to date, neither experimentally nor theoretically. As such, it may not be a-priori obvious whether such a system can be realized at all in practice. In this paper, we describe an explicit realization of the GEIT system, using non-degenerate Zeeman sublevels in alkali atoms, specifically ^{87}Rb atoms. In Section 2, we describe the Rb GEIT system in detail. In Section 3, we theoretically model the GEIT system using the density-matrix approach and calculate the quantum noise limited sensitivity of the WLC-SR detector incorporating this system in the WLC. In Section 4, we summarize the results and present an outlook for future studies.

---

* Corresponding author.
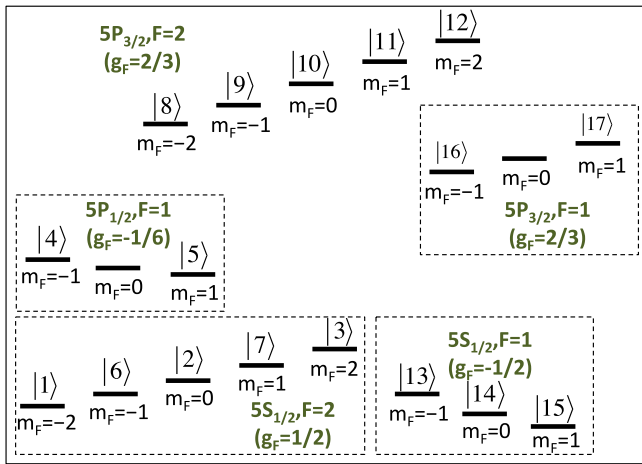*E-mail address:* minchuanzhou2013@u.northwestern.edu (M. Zhou).

Fig. 1. 17 non-degenerate Zeeman sublevels in ^{87}Rb atoms used for realizing the GEIT system.

2. Description of the GEIT system using ^{87}Rb

We use the 17 non-degenerate Zeeman sublevels in ^{87}Rb atoms as shown in Fig. 1 for realizing the GEIT system. The optical excitation scheme is illustrated schematically in Fig. 2(a). The five levels constituting the M-type system as illustrated in Fig. 2(b) are represented by the following Zeeman sub-levels: $|1\rangle = 5S_{1/2}, F = 2, m_F = -2$, $|2\rangle = 5S_{1/2}, F = 2, m_F = 0, |3\rangle = 5S_{1/2}, F = 2, m_F = 2, |4\rangle = 5P_{1/2}, F = 1, m_F = -1$, and $|5\rangle = 5P_{1/2}, F = 1, m_F = 1$. These states belong to only two hyperfine levels: $\{5S_{1/2}, F = 2\}$ and $\{5P_{1/2}, F = 1\}$. However, in order to ensure that these levels produce the desired GEIT effect, it is also necessary to make use of additional hyperfine levels, namely $\{5S_{1/2}, F = 1\}$, $\{5P_{3/2}, F = 1\}$, and $\{5P_{3/2}, F = 2\}$. For the parameters and conditions considered here, as explained in detail later, the effect of the remaining hyperfine levels within the D_1 and the D_2 transitions can be ignored.

In order to lift the degeneracy between the Zeeman sublevels, we assume the application of a moderate magnetic field along the quantization axis. The Lande g_F-factors for each of the five hyperfine levels are shown in Fig. 1. For a magnetic field strength B (in Gauss), the energy shift for a Zeeman sublevel with quantum number m_F is given by $1.4g_F m_F B$ MHz. The strength of B is to be kept low enough so that

the Zeeman splitting between adjacent m_F levels is small compared to the hyperfine splitting within the corresponding fine structure.

The transitions $|1\rangle–|4\rangle$, $|2\rangle–|4\rangle$ and $|3\rangle–|5\rangle$ are coupled by the pump fields Ω_1 (σ^+-polarized), Ω_2 (σ^--polarized), and Ω_4 (σ^--polarized), respectively, while the transition $|2\rangle–|5\rangle$ is coupled by the probe field Ω_3 (σ^+-polarized). The pump fields and the probe field are all below resonance. (We assume the use of cold atoms, so that Doppler broadening is neglected.)

The optical pumping beams applied on the D_2 transition are also shown in Fig. 2(a). The two π-polarized lights (π_1 and π_2) coupling the $F = 1, m_F = \pm 1$ ground states to the $F = 1, m_F = \pm 1$ states in the $5P_{3/2}$ manifold and the π-polarized light (π_3) coupling the $F = 1, m_F = 0$ ground state to the $F = 2, m_F = 0$ state in the $5P_{3/2}$ manifold ensure that no atoms can get trapped in the $5S_{1/2}, F = 1$ state. The σ^+-polarized and σ^--polarized optical pumping beams ensure that atoms would not get trapped in the $5S_{1/2}, F = 2, m_F = \pm 1$ states (levels $|6\rangle$ and $|7\rangle$). Furthermore, in the absence of the beams that excite the GEIT transitions, these optical pumping beams would send all the atoms into the ground states $|1\rangle$ and $|3\rangle$, thus producing the population imbalance necessary for Raman gain.

The detunings of the pump fields and the probe field are denoted by δ_j ($j = 1, 2, 3, 4$). The detunings of the pump fields Ω_1 and Ω_2 are chosen to balance the differential light shift experienced by levels $|1\rangle$ [$\Omega_1^2/(4\delta_1)$] and $|2\rangle$ [$\Omega_2^2/(4\delta_2) + \Omega_3^2/(4\delta_3)$], so that the left leg $|1\rangle–|4\rangle–|2\rangle$ is two-photon resonant. For the other leg, $|2\rangle–|5\rangle–|3\rangle$, we define $\delta_3 = \delta_{30} + \Delta$ where $\Delta = 0$ corresponds to the two-photon resonant condition of the right leg, while taking into account the light shift of level $|3\rangle$ caused by Ω_4 [$\Omega_4^2/(4\delta_4)$], as well as the light shift of level $|2\rangle$ mentioned above. Due to the Raman-type population inversion between levels $|1\rangle$ and $|2\rangle$, Ω_2 will experience Raman gain in the presence of Ω_1. Similarly, Ω_3 will experience Raman gain in the presence of Ω_4 due to the population inversion between levels $|3\rangle$ and $|2\rangle$. However, when both legs are two photon resonant, the Raman transition amplitude from $|1\rangle$ to $|2\rangle$ can cancel that from $|3\rangle$ to $|2\rangle$, which is similar to the dark state in the electromagnetically induced transparency.

This system can be used as the NDM in the white-light-cavity signal-recycling (WLC-SR) [8,10] interferometric gravitational wave detector, which is shown schematically in Fig. 3. Here we use a Michelson interferometer with arm cavities and dual recycling, which is the scheme used by the advanced Laser Interferometric Gravitational wave Observatory (aLIGO) [12]. The signal recycling (SR) cavity, consisting of the SR mirror and the front mirrors of the arm cavities, forms a coupled cavity with the end mirrors of the arm cavities. With different choices of the length of the SR cavity (L_{SRC}), the interferometer can

(a)   (b)
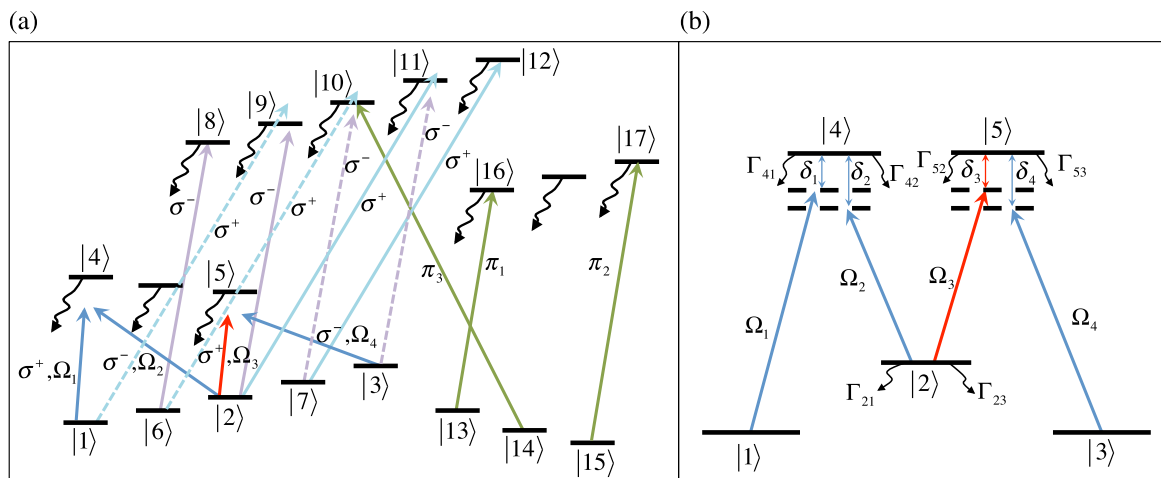

Fig. 2. (a) Illustration of the optical excitation scheme for realizing the M-type gain with electromagnetically induced transparency (GEIT) system using ^{87}Rb atoms; (b) Schematic illustration of the effective five-level system that results from these interactions. The decay rates for state $|2\rangle$, as shown in Fig. 2(b), are due to the optical pumping via its coupling to the $5P_{3/2}, F = 2$ hyperfine state.
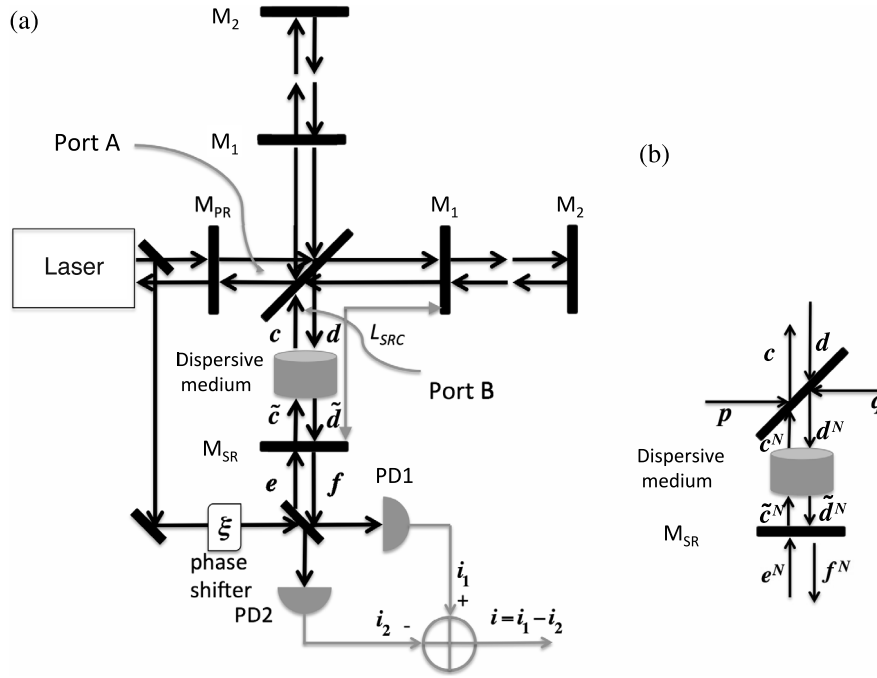
Fig. 3. (a) WLC-SR design. A dispersive medium realized using ^{87}Rb atoms is inserted in the SR cavity. Here the input field is denoted by e and the output field is denoted by f. (b) The SR cavity where the QN from the dispersive medium is modeled by inserting a beam splitter with power reflectivity R_{BS} and transmissivity T_{BS}. Here p and q denote the vacuum noises that leak into the system.

operate in different modes [11]. When $\varphi_{SRC} = k_c L_{SRC}(\bmod 2\pi) = \pi/2$, the interferometer operates in the extreme resonant-sideband-extraction configuration. The case $\varphi_{SRC} = k_c L_{SRC}(\bmod 2\pi) = 0$ is called extreme signal-recycling configuration. The scheme where $\varphi_{SRC} \neq 0$ or $\pi/2$ is called detuned signal recycling, where a certain sideband frequency is resonant in the coupled cavity, which is the operating mode for the WLC-SR scheme considered here. An NDM is inserted in the SR cavity in order to compensate the phase variation as the frequency varies. Current LIGO operates at 1064 nm, which is different from the probe frequency in our system. However, future LIGO may operate at a wavelength consistent with this system. In order to use this system in LIGO, the interferometer needs to be illuminated with a circularly (σ^+) polarized laser instead of the current linearly polarized laser, at ∼795 nm. The pump fields corresponding to Ω_1, Ω_2 and Ω_4 have to be generated by splitting a part of the main laser, followed by frequency shifting using acoustic-optic modulators, for example. The optical pumping beams at ∼780 nm can be generated from an independent, separate laser.

3. Theoretical model of the GEIT system

We develop a full-blown model that takes into account all the relevant Zeeman sublevels participating in the process, using the density-matrix approach. The three π polarized fields are assumed to be resonant with the corresponding transitions and have Rabi frequencies of $\Omega_{p,\pi k}(k = 1, 2, 3)$. The σ^+-polarized and σ^--polarized fields applied on the D2 transition each couples four transitions. We express all the Rabi frequencies as multiples of the Rabi frequency for the transition with the smallest dipole moment, since the Rabi frequency of each transition is proportional to its corresponding dipole moment matrix element [13]. For example, we write the Rabi frequencies of the transitions $|6\rangle$–$|8\rangle$, $|2\rangle$–$|9\rangle$, $|7\rangle$–$|10\rangle$, and $|3\rangle$–$|11\rangle$, respectively, as:

$$\Omega_1^- = -\Omega_{p,\sigma-}, \qquad \Omega_2^- = -\sqrt{\frac{3}{2}}\Omega_{p,\sigma-}, \qquad \Omega_3^- = -\sqrt{\frac{3}{2}}\Omega_{p,\sigma-},$$
$$\Omega_4^- = -\Omega_{p,\sigma-}. \tag{1}$$

Similarly, we write the Rabi frequencies of the transitions $|7\rangle$–$|12\rangle$, $|2\rangle$–$|11\rangle$, $|6\rangle$–$|10\rangle$, and $|1\rangle$–$|9\rangle$, respectively, as:

$$\Omega_1^+ = \Omega_{p,\sigma+}, \qquad \Omega_2^+ = \sqrt{\frac{3}{2}}\Omega_{p,\sigma+}, \qquad \Omega_3^+ = \sqrt{\frac{3}{2}}\Omega_{p,\sigma-},$$
$$\Omega_4^+ = \Omega_{p,\sigma+}. \tag{2}$$

We assume that the σ^--polarized light is resonant with the $|6\rangle$–$|8\rangle$ transition. As a result, the other three transitions are below resonance and the detunings for the four transitions are $\delta_l^- = 0.23B(l - 1)$ MHz, where $l = 2, 3, 4$ correspond to the $|2\rangle$–$|9\rangle$, $|7\rangle$–$|10\rangle$, and $|3\rangle$–$|11\rangle$ transitions, respectively. If we consider each transition as an effective two-level system, then the excitation at the higher level is

$$\rho_{ll}^- = \frac{(\Omega_l^-)^2}{\Gamma^2 + 2(\Omega_l^-)^2 + 4(\delta_l^-)^2}, \tag{3}$$

which is on the order of 10^{-6} if we take $\Omega_{p,\sigma-} \approx 0.038$ MHz and $\Gamma = 6$ MHz, and decreasing with increasing value of l. Therefore, for simplicity, we keep the $|2\rangle$–$|9\rangle$ interactions, but neglect the $|7\rangle$–$|10\rangle$ and $|3\rangle$–$|11\rangle$ transitions (amounting to setting $\Omega_3^- = \Omega_4^- = 0$). Similarly, we assume that the σ^+-polarized light is resonant with the $|7\rangle$–$|12\rangle$ transition and neglect the couplings of the σ^+-polarized light with the $|1\rangle$–$|9\rangle$ and $|6\rangle$–$|10\rangle$ transitions (amounting to setting $\Omega_3^+ = \Omega_4^+ = 0$), while keeping the $|2\rangle$–$|11\rangle$ coupling. We will show later in this paper that the QN limited sensitivity of the WLC-SR using this system does not change significantly when the coupling of the σ^--polarized light to the $|7\rangle$–$|10\rangle$ transition and that of the σ^+-polarized light to the $|6\rangle$–$|10\rangle$ transition are included [14].

For the fields that couple the Zeeman sublevels within the $\{5S_{1/2}, F = 2\}$ manifold to those within the $\{5P_{1/2}, F = 1\}$ manifold, there are four different laser beams with different frequencies. These beams produce additional coupling beyond those shown in Fig. 2. For example, the σ^+-polarized beam with Rabi frequency Ω_3 would excite the $|1\rangle$–$|4\rangle$ transition as well. This creates a situation where the $|1\rangle$–$|4\rangle$ transition is excited simultaneously by fields at two different frequencies. Under this condition, the Hamiltonian would retain a time dependent component after the rotating wave transformation, and the resulting solution of the density matrix would have terms that are

harmonics of the frequency corresponding to this time dependent term. Furthermore, similar effect would occur for the |2⟩–|4⟩, |2⟩–|5⟩, and |3⟩–|5⟩ transitions as well, making it exceedingly difficult to simulate the behavior of the system more exactly. To circumvent this problem, we have only considered interactions that couple the Zeeman sublevels within the $\{5S_{1/2}, F = 2\}$ manifold via two-photon resonances. Since, in steady state, most of the populations are in levels |1⟩ and |3⟩ within this manifold, such an approximation is justified. In the same vein, we have ignored all couplings of levels |6⟩ and |7⟩ caused by these four beams, since optical pumping moves atom out of these two states.

The $\{5P_{1/2}, F = 2\}$ manifold is not shown in the scheme in Fig. 2. For example, the pump field Ω_1 couples to not only the transition from level |1⟩ to level |4⟩ in the $\{5P_{1/2}, F = 1\}$ manifold, but also the transition from level |1⟩ to $|5P_{1/2}, F = 2, m_F = -1\rangle$ in the $\{5P_{1/2}, F = 2\}$ manifold, with a Rabi frequency of Ω_1' and a detuning of δ_1'. This additional coupling will introduce an additional light shift $\Omega_1'^2/(4\delta_1')$ to level |1⟩. It can be taken into account using an effective Rabi frequency $\tilde{\Omega}_1$ which satisfies the condition that $\tilde{\Omega}_1^2/(4\delta_1) = \Omega_1^2/(4\delta_1) + \Omega_1'^2/(4\delta_1')$. Similarly, we can use effective Rabi frequencies for the rest of the pumps fields and the probe field Ω_j ($j = 2, 3, 4$) to take into account the light shifts induced by the additional couplings to the $\{5P_{1/2}, F = 2\}$ manifold. Thus, the $\{5P_{1/2}, F = 2\}$ manifold can be incorporated by effective Rabi frequencies for the pump and probe fields.

The decay of the upper levels to the ground states are included using the decay rates Γ_m ($m = 4, 5, 8, 9, 10, 11, 12, 16, 17$). The time-independent Hamiltonian after the rotating wave approximation (RWA) and the rotating wave transformation can be written as (setting $\hbar = 1$):

$$\tilde{H}_{1,1} = 0, \qquad \tilde{H}_{2,2} = \delta_1 - \delta_2, \qquad \tilde{H}_{3,3} = \delta_1 - \delta_2 + \delta_3 - \delta_4,$$
$$\tilde{H}_{4,4} = \delta_1 - i\Gamma_4/2, \qquad \tilde{H}_{5,5} = \delta_1 - \delta_2 + \delta_3 - i\Gamma_5/2, \tag{4}$$

$$\tilde{H}_{6,6} = \Delta_{B1}, \qquad \tilde{H}_{7,7} = 5\Delta_{B1} - 4\Delta_{B3}, \qquad \tilde{H}_{8,8} = \Delta_{B1} - i\Gamma_8/2,$$
$$\tilde{H}_{9,9} = \delta_1 - \delta_2 - \Delta_{B1} + \Delta_{B3} - i\Gamma_9/2, \tag{5}$$

$$\tilde{H}_{10,10} = 3\Delta_{B1} - 2\Delta_{B3} - i\Gamma_{10}/2,$$
$$\tilde{H}_{11,11} = \delta_1 - \delta_2 + \Delta_{B1} - \Delta_{B3} - i\Gamma_{11}/2,$$
$$\tilde{H}_{12,12} = 5\Delta_{B1} - 4\Delta_{B3} - i\Gamma_{12}/2, \tag{6}$$

$$\tilde{H}_{13,13} = 3\Delta_{B1} - 2\Delta_{B3} - \Delta_{B4}, \qquad \tilde{H}_{14,14} = 3\Delta_{B1} - 2\Delta_{B3},$$
$$\tilde{H}_{15,15} = 3\Delta_{B1} - 2\Delta_{B3} + \Delta_{B4}, \tag{7}$$

$$\tilde{H}_{16,16} = 3\Delta_{B1} - 2\Delta_{B3} - \Delta_{B4} - i\Gamma_{16}/2,$$
$$\tilde{H}_{17,17} = 3\Delta_{B1} - 2\Delta_{B3} + \Delta_{B4} - i\Gamma_{17}/2, \tag{8}$$

$$\tilde{H}_{1,4} = \Omega_1/2 = \tilde{H}_{4,1}, \qquad \tilde{H}_{2,4} = \Omega_2/2 = \tilde{H}_{4,2},$$
$$\tilde{H}_{2,5} = \Omega_3/2 = \tilde{H}_{5,2}, \qquad \tilde{H}_{3,5} = \Omega_4/2 = \tilde{H}_{5,3}, \tag{9}$$

$$\tilde{H}_{10,14} = \Omega_{p,\pi3}/2 = \tilde{H}_{14,10}, \qquad \tilde{H}_{13,16} = \Omega_{p,\pi1}/2 = \tilde{H}_{16,13},$$
$$\tilde{H}_{15,17} = \Omega_{p,\pi2}/2 = \tilde{H}_{17,15}, \tag{10}$$

$$\tilde{H}_{6,8} = \tilde{H}_{8,6} = \Omega_1^-/2, \qquad \tilde{H}_{2,9} = \tilde{H}_{9,2} = \Omega_2^-/2,$$
$$\tilde{H}_{7,10} = \tilde{H}_{10,7} = \Omega_3^-/2, \qquad \tilde{H}_{3,11} = \tilde{H}_{11,3} = \Omega_4^-/2, \tag{11}$$

$$\tilde{H}_{7,12} = \tilde{H}_{12,7} = \Omega_1^+/2, \qquad \tilde{H}_{2,11} = \tilde{H}_{11,2} = \Omega_2^+/2,$$
$$\tilde{H}_{6,10} = \tilde{H}_{10,6} = \Omega_3^+/2, \qquad \tilde{H}_{1,9} = \tilde{H}_{9,1} = \Omega_4^+/2, \tag{12}$$

where $\Delta_{B1} = (0.7B)$ MHz, $\Delta_{B2} = (-0.23B)$ MHz, $\Delta_{B3} = (0.93B)$ MHz, $\Delta_{B4} = (-0.7B)$ MHz, and $\Delta_{B5} = (0.93B)$ MHz are the Zeeman splitting between adjacent m_F levels in the five hyperfine levels $\{5S_{1/2}, F = 2\}$,

$\{5P_{1/2}, F = 1\}$, $\{5P_{3/2}, F = 2\}$, $\{5S_{1/2}, F = 1\}$, and $\{5P_{3/2}, F = 1\}$, respectively. The remaining terms of $\tilde{H}$ are all zero. The equation of evolution for the density operator can be expressed as

$$\frac{\partial \tilde{\rho}}{\partial t} = -\frac{i}{\hbar}(\tilde{H}\tilde{\rho} - \tilde{\rho}\tilde{H}^*) + \left(\frac{\partial \tilde{\rho}}{\partial t}\right)_{source}, \tag{13}$$

where the second term represents the influx of atoms into a state due to decay from another state [15]. The decay rates between any two Zeeman sub-levels are proportional to the squares of the dipole moment matrix elements. As a result, the source terms are expressed as

$$\left(\frac{\partial \tilde{\rho}_{1,1}}{\partial t}\right)_{source} = \frac{\Gamma_4}{2}\tilde{\rho}_{4,4} + \frac{\Gamma_8}{3}\tilde{\rho}_{8,8} + \frac{\Gamma_9}{6}\tilde{\rho}_{9,9} + \frac{\Gamma_{16}}{10}\tilde{\rho}_{16,16}, \tag{14}$$

$$\left(\frac{\partial \tilde{\rho}_{2,2}}{\partial t}\right)_{source} = \frac{\Gamma_4}{12}\tilde{\rho}_{4,4} + \frac{\Gamma_5}{12}\tilde{\rho}_{5,5} + \frac{\Gamma_9}{4}\tilde{\rho}_{9,9} + \frac{\Gamma_{11}}{4}\tilde{\rho}_{11,11}$$
$$+ \frac{\Gamma_{16}}{60}\tilde{\rho}_{16,16} + \frac{\Gamma_{17}}{60}\tilde{\rho}_{17,17}, \tag{15}$$

$$\left(\frac{\partial \tilde{\rho}_{3,3}}{\partial t}\right)_{source} = \frac{\Gamma_5}{2}\tilde{\rho}_{5,5} + \frac{\Gamma_{11}}{6}\tilde{\rho}_{11,11} + \frac{\Gamma_{12}}{3}\tilde{\rho}_{12,12} + \frac{\Gamma_{17}}{10}\tilde{\rho}_{17,17}, \tag{16}$$

$$\left(\frac{\partial \tilde{\rho}_{6,6}}{\partial t}\right)_{source} = \frac{\Gamma_4}{4}\tilde{\rho}_{4,4} + \frac{\Gamma_8}{6}\tilde{\rho}_{8,8} + \frac{\Gamma_9}{12}\tilde{\rho}_{9,9} + \frac{\Gamma_{10}}{4}\tilde{\rho}_{10,10} + \frac{\Gamma_{16}}{20}\tilde{\rho}_{16,16}, \tag{17}$$

$$\left(\frac{\partial \tilde{\rho}_{7,7}}{\partial t}\right)_{source} = \frac{\Gamma_5}{4}\tilde{\rho}_{5,5} + \frac{\Gamma_{10}}{4}\tilde{\rho}_{10,10} + \frac{\Gamma_{11}}{12}\tilde{\rho}_{11,11}$$
$$+ \frac{\Gamma_{12}}{6}\tilde{\rho}_{12,12} + \frac{\Gamma_{17}}{20}\tilde{\rho}_{17,17}, \tag{18}$$

$$\left(\frac{\partial \tilde{\rho}_{13,13}}{\partial t}\right)_{source} = \frac{\Gamma_4}{12}\tilde{\rho}_{4,4} + \frac{\Gamma_8}{2}\tilde{\rho}_{8,8} + \frac{\Gamma_9}{4}\tilde{\rho}_{9,9}$$
$$+ \frac{\Gamma_{10}}{12}\tilde{\rho}_{10,10} + \frac{5}{12}\Gamma_{16}\tilde{\rho}_{16,16}, \tag{19}$$

$$\left(\frac{\partial \tilde{\rho}_{14,14}}{\partial t}\right)_{source} = \frac{\Gamma_4}{12}\tilde{\rho}_{4,4} + \frac{\Gamma_5}{12}\tilde{\rho}_{5,5} + \frac{\Gamma_9}{4}\tilde{\rho}_{9,9} + \frac{\Gamma_{10}}{3}\tilde{\rho}_{10,10}$$
$$+ \frac{\Gamma_{11}}{4}\tilde{\rho}_{11,11} + \frac{5}{12}\Gamma_{16}\tilde{\rho}_{16,16} + \frac{5}{12}\Gamma_{17}\tilde{\rho}_{17,17}, \tag{20}$$

$$\left(\frac{\partial \tilde{\rho}_{15,15}}{\partial t}\right)_{source} = \frac{\Gamma_5}{12}\tilde{\rho}_{5,5} + \frac{\Gamma_{10}}{12}\tilde{\rho}_{10,10} + \frac{\Gamma_{11}}{4}\tilde{\rho}_{11,11}$$
$$+ \frac{\Gamma_{12}}{2}\tilde{\rho}_{12,12} + \frac{5}{12}\Gamma_{17}\tilde{\rho}_{17,17}. \tag{21}$$

These equations are solved in steady state. Scanning the probe detuning δ_3, we plot in Fig. 4 the real and imaginary parts of the susceptibility for the probe field Ω_3 normalized by the number density n, which is $\chi/n = -\hbar c \Gamma_5^2 \tilde{\rho}_{52}/(I_{sat}\Omega_3)$. Here the saturation intensity is $I_{sat} = I_{cyc}(d_{cyc}/d_{2-5})^2$, where $I_{cyc} = 16.6933$ W/m² is the saturation intensity for the cycling transition $|F = 2, m_F = 2\rangle \rightarrow |F = 3, m_F = 3\rangle$, and d_{cyc} and d_{2-5} are the matrix elements for the cycling transition and the $|2\rangle \rightarrow |5\rangle$ transition, respectively. A magnetic field of 40 Gauss is used. The Rabi frequencies of the pump fields are $\Omega_1 = 0.6$ MHz, $\Omega_2 = 18$ MHz, and $\Omega_4 = 12$ MHz, respectively, and the Rabi frequency of the probe field is $\Omega_3 = 60$ Hz. The detunings of the pump fields and the probe field are all set to be ~2.23 GHz. The Rabi frequencies of the optical pumping beams are $\Omega_{p,\pi1} = \Omega_{p,\pi2} = \Omega_{p,\pi3} = 0.06$ MHz and $\Omega_{p,\sigma-} = \Omega_{p,\sigma+} \approx 0.038$ MHz, respectively. The decay rate of the upper levels is assumed to be $\Gamma_m = 6$ MHz. We show that a negative dispersion is produced in Fig. 4(a) and the transmission profile with a dip on top of a broad gain is plotted in Fig. 4(b).

The QN limited sensitivity for the GW signal in the WLC-SR scheme in Fig. 3 is calculated using the input–output relation between the principal noise input $e = (e_1, e_2)^T$ from Port B and the signal and noise output $f = (f_1, f_2)^T$ [8]. Here we follow the two-photon formalism developed by Caves and Schumaker [16,17] to represent the fields as the amplitudes of the two-photon modes.
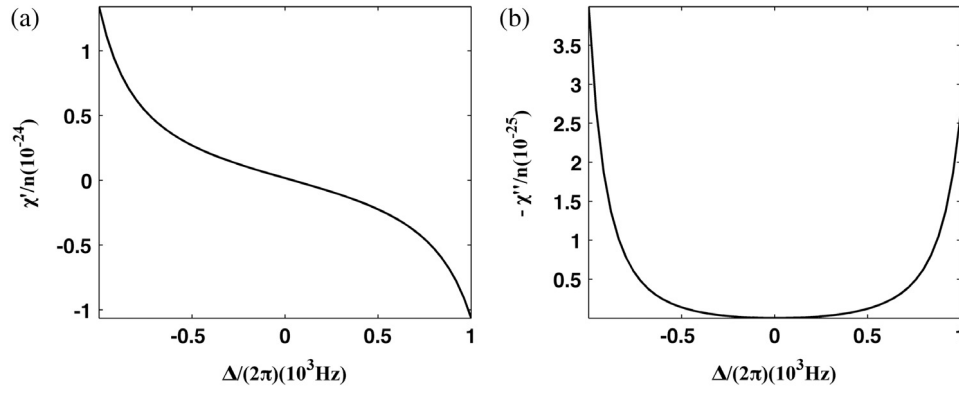
Fig. 4. (a) Imaginary and (b) real parts of χ/n (χ is the susceptibility and n is the number density of Rb atoms) as a function of detuning $\Delta = \omega - \omega_0$ in the ^{87}Rb based GEIT system. Here ω_0 is the frequency corresponding to the dip in the transmission. The parameters used in the GEIT system is $B = 40$ Gauss, $\Omega_1 = 0.6$ MHz, $\Omega_2 = 18$ MHz, $\Omega_3 = 60$ Hz, $\Omega_4 = 12$ MHz, $\delta_1 \cong \delta_2 \cong \delta_3 \cong \delta_4 \cong 2.23$ GHz, $\Omega_{p,\pi1} = \Omega_{p,\pi2} = \Omega_{p,\pi3} = 0.06$ MHz, $\Omega_{p,\sigma-} = \Omega_{p,\sigma+} \cong 0.038$ MHz, and $\Gamma_m = 6$ MHz.

In order to calculate the QN in this GEIT system accurately, the ME approach should be used [10]. However, this is a very challenging task for the highly complex system being considered here, without assurance of success. To see why, we first recall briefly the relevant aspects of the process involved in developing and solving the MEs for calculating QN. To this end, we point to Ref. [10], where we calculated the QN for the five-level GEIT system using the ME approach. We started with the equations of motion for the atom-field density operator ρ_{a-f} in the interaction picture, taking into account the decay processes [Eq. (2) in Ref. [10]], by treating the pump fields semi-classically and treating the probe field quantum mechanically. The set of equations of motion for the 25 density matrix elements $\rho_{\alpha n,\beta n'} = \langle \alpha, n|\rho_{a-f}|\beta, n'\rangle$ [$|\alpha\rangle$ and $|\beta\rangle$ ($\alpha, \beta = 1, 2, 3, 4, 5$) represent atomic states, and $|n\rangle$ and $|n'\rangle$ represent quantum states of the probe field] in one manifold were derived. Two example equations were shown as Eqs. (124) and (125) in Ref. [10]. The complete set of equations actually consists of an (essentially) infinite number of equations since the values of $\{n, n'\}$ extend from zero to (essentially) infinity. Similar to the case of the two-level atomic system as illustrated in Fig. 2 of Ref. [10], the couplings between the matrix elements exist both within a given manifold and between different manifolds. We used the steady state solutions of the semiclassical equations involving the atomic states only to make the approximations [as shown in Eqs. (126) and (127)] necessary to remove the coupling between different manifolds. Considering the 25 matrix elements for the density matrix as a vector, the equations of motion for each manifold can be written in a matrix form [as seen in Eq. (21) in Ref. [10]] where the coefficient matrix M has a dimension of 25×25, with 625 matrix elements. Due to the complexity of the system, we cannot get an analytical solution to these 25 equations, unlike the case for the two-level system shown in Eqs. (25) and (26) of Ref. [10]. The solution of the density matrix elements $\rho_{\alpha n,\beta n'}$ is a linear combination of the matrix elements $\tilde{\rho}_{n,n'} = \langle n|\tilde{\rho}|n'\rangle$ of the field density operator $\tilde{\rho} = Tr_{atom}(\rho_{a-f})$. For the 5-level system, the values of the coefficients for the matrix elements $\tilde{\rho}_{n,n'}$ of the field density operator in the solutions of $\rho_{\alpha n,\beta n'}$ were calculated numerically for each combination of parameters. These solutions were then plugged into the equation of motion for the field density operator [Eq. (4) in Ref. [10]], from which we derived the equations of motion for the relevant moments of the annihilation and creation operators of the field [Eq. (5) in Ref. [10]]. The QN in the quadratures of the field [X_θ in Eq. (41) of Ref. [10]] were calculated from these equations.

In the case of the Rb GEIT system considered in this paper, with 17 energy levels and many optical pumping beams, there are $17^2 = 289$ equations of motions for the matrix elements, and therefore $17^4 = 83521$ elements in the coefficient matrix M, in each manifold. It will be very difficult and time consuming to decouple different manifolds and to solve for the coefficients numerically for each combination of parameters. More importantly, it is not at all clear a priori that the resulting equations can be solved with enough accuracy. This is
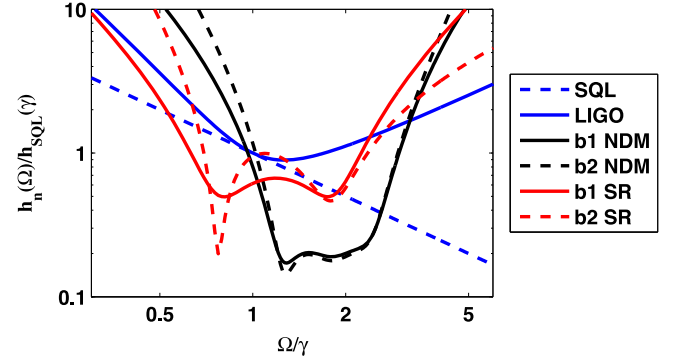

Fig. 5. Log–log plot of the normalized quantum noise $h_n(\Omega)/h_{SQL}(\gamma)$ of the GW detector versus Ω/γ for the first quadrature b1 and second quadrature b2, following the two-photon formalism developed in Refs. [16,17]. Here $h_n(\Omega)$ is the square root of the noise spectral density for the GW signal at a sideband frequency Ω, $h_{SQL}(\gamma)$ is the standard quantum limit for GW detection at a sideband frequency $\Omega = \gamma$, where $\gamma/(2\pi) = 100$ Hz is the half bandwidth of the arm cavity of the detector. The black curves represent the quantum noise for the WLC-SR using the GEIT system as the NDM, in which we use the same set of parameters as in Fig. 4 and a density-length product of 1.25×10^{18} m^{-2}. The red curves represent the quantum noise for the GW detector with SR. The noise curve for LIGO and the standard quantum limit (SQL) curve are plotted in blue. For additional details underlying the notations used here, see, for example, Ref. [8] or Ref. [11]. The noise curves for the WLC-SR scheme shows an enhancement in sensitivity-bandwidth product by a factor of ~19 compared to the curve for the SR configuration with the highest sensitivity (b2 quadrature). Since the application of the Caves model to GEIT implies an overestimation of the enhancement factor by as much as 11%, the lower bound on the enhancement factor is ~17.

because decoupling the infinite number of manifolds (corresponding to photon numbers) can only be done by making use of the steady state solution of the semiclassical equations involving the atomic states only, as mentioned above. Whether the use of this steady state solution for decoupling the photon manifolds is valid or not depends on the complexity of the system. In the cases we have studied in Ref. [9], we verified the validity of this approximation by comparing the response of the decoupled system to that of the semi-classical system. For two, three, and four level cases, we were able to compare the results analytically. However, for the five level case, we were able to carry out these comparisons only numerically. In the 17 level case, we will also have to carry out the comparison numerically. However, because of the much larger number of parameters involved, it would be very difficult to verify the range of these parameters for which this approximation is valid. If it turns out to be the case that the validity of this approximation cannot be established clearly for the 17 level system, then we will have to conclude that the ME for such a system simply cannot be solved (due to the fact that it couples an infinite number of manifolds). Thus, whether the ME approach can be used to determine the QN for the 17-level system remains an open question, subject to future studies.
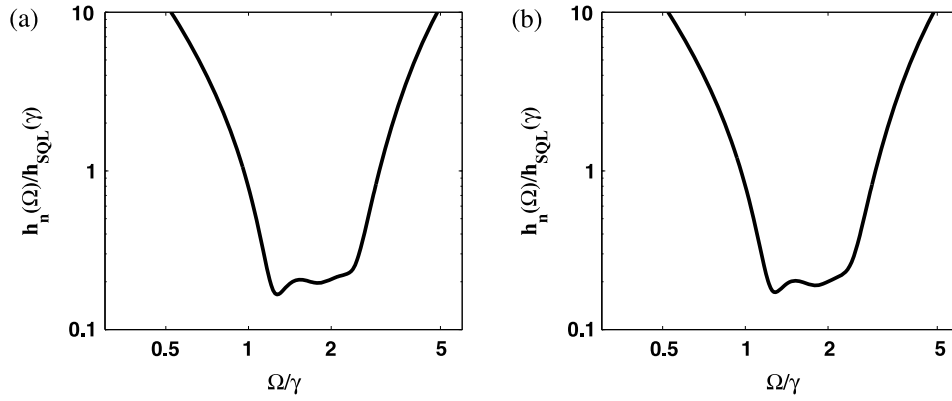
Fig. 6. Log–log plots of the normalized quantum noise $h_n(\Omega)/h_{SQL}(\gamma)$ versus Ω/γ for the first quadrature b1 for the WLC-SR scheme using the GEIT system with (a) and without (b) taking into account the coupling of the σ^--polarized light to the $|7\rangle$–$|10\rangle$ transition and that of the σ^+-polarized light to the $|6\rangle$–$|10\rangle$ transition.

It should be noted that the GEIT system is a phase-insensitive linear amplifier, and that in some phase-insensitive linear amplifiers or attenuators, the ME approach agrees closely with the Caves model [18,19], as we have also shown earlier in Ref. [10]. In one of the two cases of the five-level GEIT system considered in Ref. [8] where we get an enhancement factor of 17.66 in the sensitivity-bandwidth product, the results predicted by ME and Caves model differ by ∼11%, while in the other case where the enhancement factor is 16.55 the results differ by less than 0.2%. Thus, it is reasonable to assume that the enhancement in the sensitivity bandwidth product calculated by using the Caves model for a GEIT system is likely to be over-estimated by a factor on the order ranging from 1.002 to 1.11. As such, we use the Caves model to determine the QN due to the amplification from the GEIT system. We model the QN by placing inside the WLC a beam splitter [BS, as shown in Fig. 3(b)] that has a power reflectivity $T_{BS} = g$ and power transmissivity of $R_{BS} = |g - 1|$, from which the vacuum fields can leak into the system from the outside. We write the input–output relation for the BS as

$$c = \sqrt{T_{BS}}c^N + \sqrt{R_{BS}}p, \qquad d^N = \sqrt{T_{BS}}d - \sqrt{R_{BS}}q. \qquad (22)$$

Using the same method as in Sec. III in Ref. [8], we plot the resulting QN curves of the WLC-SR scheme in Fig. 5, which shows an enhancement in sensitivity-bandwidth product by a factor of ∼19 compared to the curve for the GW detector with signal recycling (SR) configuration with the highest sensitivity (shown as red dashed curve). If we employ the upper bound (1.11) of the overestimation factor, then the actual enhancement factor would be ∼17. Here we use the density-length product of $nl = 1.25 \times 10^{18}$ m^{-2} (n is the number density of Rb atoms and l is the length of the NDM). For $l = 1$ m, the number density required is $n = 1.25 \times 10^{18}$ m^{-3}. Such a number density is achievable using a holographically shaped dark spontaneous-force optical trap (SPOT) for a dark core radius of around 6 mm [20], and an atom cloud diameter of about 0.6 mm. Due to the physical constraints imposed by the trap geometry, these clouds cannot be placed right next to each other. Instead, one can place the traps apart with a separation of, for example, 6 cm between adjacent ones. This will represent a filling factor of 1%. Thus, in order to reach the effective value of nl noted above, the actual length covered by the array of traps has to be ∼100 m. In order to accommodate this configuration, the distance between the beam splitter and M_{SR} (in Fig. 3) has to be increased to a value of ∼100 m. We have verified that such a change in the relative position of the SR mirror does not affect the dynamics of the WLC-SR scheme to any noticeable degree. Finally, note that the size of the signal beam must be small than ∼0.6 mm at the trap location. To accommodate this constraint, the dark port output of the beam splitter will first be reduced to a diameter of ∼0.4 mm using a telescope. In addition, periodic refocusing lenses would be inserted, within the ∼100 m propagation path, to ensure that the beam diameter does not exceed ∼0.5 mm. While it would be a

challenging task to implement such a system experimentally, it is by no means implausible.

Next, we consider the case where the coupling of the σ^--polarized light to the $|7\rangle$–$|10\rangle$ transition and that of the σ^+-polarized light to the $|6\rangle$–$|10\rangle$ transition are included by taking

$$\Omega_3^- = -\sqrt{\frac{3}{2}}\Omega_{p,\sigma-}, \qquad \Omega_3^+ = \sqrt{\frac{3}{2}}\Omega_{p,\sigma-}. \qquad (23)$$

For this case, we again calculate the resulting dispersion and the quantum noise curves for the WLC-SR scheme. As a comparison, we show in Fig. 6 the sensitivity curves for the first quadrature, with and without taking into account the above couplings, respectively. In this case, the difference is very small. Similar agreement is seen for the second quadrature as well (not shown). This result justifies our assumption that the $|7\rangle$–$|10\rangle$ and the $|6\rangle$–$|10\rangle$ coupling can be neglected. In addition, it justifies the assumption that the $|1\rangle$–$|9\rangle$ and the $|3\rangle$–$|11\rangle$ coupling can also be neglected.

4. Conclusion and future plan

We have presented an explicit realization of the five-level GEIT system, which shows a negative dispersion and also an EIT dip superimposed on a broad gain profile, using non-degenerate Zeeman sublevels in ^{87}Rb atoms centered around 795 nm. The current LIGO operates at 1064 nm but future LIGO may operate at a wavelength that is consistent with this atomic system. Moreover, the interferometer needs to be illuminated with a circularly (σ^+) polarized laser instead of the current linearly polarized laser used in a LIGO. In that case, the GEIT system can in principle be incorporated as the negative dispersion medium in the WLC-SR scheme of gravitational wave detector. Estimating its quantum noise using the Caves model and considering an overestimation of the enhancement factor by as much as ∼11%, we determine the quantum-noise-limited enhancement in the sensitivity-bandwidth to be ∼17.

In the future, we will realize this GEIT system experimentally, and verify that its gain and dispersion profile agrees with the theoretical prediction.

Acknowledgments

References

[1] R.H. Rinkleff, A. Wicht, The concept of white light cavities using atomic phase coherence, Phys. Scr. T118 (2005) 85–88.
[2] A. Wicht, R.H. Rinkleff, L.S. Molella, K. Danzmann, Comparative study of anomalous dispersive transparent media, Phys. Rev. A 66 (2002) 063815.

[3] A. Rocco, A. Wicht, R.H. Rinkleff, K. Danzmann, Anomalous dispersion of transparent atomic two- and three-level ensembles, Phys. Rev. A 66 (2002) 053804.

[4] A. Wicht, M. Muller, R.H. Rinkleff, A. Rocco, K. Danzmann, Experimental demonstration of negative dispersion without absorption, Opt. Commun. 179 (2000) 107–115.

[5] G.S. Pati, M. Salit, K. Salit, M.S. Shahriar, Demonstration of a tunable-bandwidth white light interferometer using anomalous dispersion in atomic vapor, Phys. Rev. Lett. 99 (2007) 133601.

[6] H.N. Yum, M. Salit, G.S. Pati, S. Tseng, P.R. Hemmer, M.S. Shahriar, Fast-light in a photorefractive crystal for gravitational wave detection, Opt. Express 16 (2008) 20448–20456.

[7] M. Salit, M.S. Shahriar, Enhancement of sensitivity-bandwidth product of interferometric gravitational wave detectors using white light cavities, J. Opt. 12 (2010) 104014.

[8] M. Zhou, Z. Zhou, S.M. Shahriar, Quantum noise limits in white-light-cavity-enhanced gravitational wave detectors, Phys. Rev. D 92 (2015) 082002.

[9] Y. Ma, H. Miao, C. Zhao, Y. Chen, Quantum noise of a white light cavity using a double-pumped gain medium, Phys. Rev. A 92 (2015) 023807.

[10] M. Zhou, Z. Zhou, S.M. Shahriar, Catastrophic breakdown of the Caves model for quantum noise in some phase insensitive linear amplifiers or attenuators based on atomic systems, Phys. Rev. A 93 (2016) 033858.

[11] A. Buonanno, Y. Chen, Quantum noise in second generation, signal-recycled laser interferometric gravitational-wave detectors, Phys. Rev. D 64 (2001) 042006.

[12] J. Aasi, et al., Advanced LIGO., Class. Quantum Gravity 32 (2015) 074001.

[13] D.A. Steck, Rubidium 87 D Line Data http://steck.us/alkalidata/rubidium87numbers.pdf.

[14] It should be noted that if we were to include the $|1\rangle$–$|9\rangle$ ($|3\rangle$–$|11\rangle$) transition, it would create a closed loop of excitations involving levels $|1\rangle, |4\rangle, |2\rangle$, and $|9\rangle$ ($|2\rangle, |5\rangle, |3\rangle$, and $|11\rangle$). In that case, and for the detuning considered here, the Hamiltonian produced after making the rotating wave transformation would remain time dependent. A computation using such a Hamiltonian leads to solutions that have multiple harmonics of the frequency corresponding to the residual time dependence in the Hamiltonian. However, since the effect of $|1\rangle$–$|9\rangle$ ($|3\rangle$–$|11\rangle$) transition is negligible for the parameters chosen, we are able to avoid this complication.

[15] M.S. Shahriar, Y. Wang, S. Krishnamurthy, Y. Tu, G.S. Pati, S. Tseng, Evolution of an N-level system via automated vectorizaition of the Liouville equations and application to optically controlled polarization rotation, J. Modern Opt. 61 (4) (2014) 351–367.

[16] C.M. Caves, B.L. Schumaker, New formalism for two-photon quantum optics. I. Quadrature phases and squeezed states, Phys. Rev. A 31 (1985) 3068.

[17] B.L. Schumaker, C.M. Caves, New formalism for two-photon quantum optics. II. Mathematical foundation and compact notation, Phys. Rev. A 31 (1985) 3093.

[18] C.M. Caves, Quantum limits on noise in linear amplifiers, Phys. Rev. D 26 (1982) 1817.

[19] Y. Yamamoto, H.A. Haus, Preparation, measurement and information capacity of optical quantum states, Rev. Mod. Phys. 58 (1986) 1001.

[20] N. Radwell, G. Walker, S. Franke-Arnold, Cold = atom densities of more than 1012 cm-3 in a holographically shaped dark spontaneous-force optical trap, Phys. Rev. A 88 (2013) 043409.